

Direct Observation of Layer-by-Layer Wear

Yifeng Liao¹ · Laurence D. Marks¹

Received: 28 January 2015 / Accepted: 6 July 2015 / Published online: 2 August 2015
© Springer Science+Business Media New York 2015

Abstract Wear at the macroscopic scale has been well documented to involve the deformation of sliding interfaces. The mechanical behavior of single asperities in sliding contact, however, is not fully understood. Classical wear mechanisms have not been necessarily substantiated by direct studies of events at the contacting interface and have often contradicted post facto investigations. Wear processes, particularly those under mild loads, are not well understood at the nanoscale to submicron scale. We report here the observation, via in situ transmission electron microscopy, of wear of $M_{23}C_6$ carbides in a CoCrMo alloy sliding against a single silicon asperity. Each slide of the asperity under a normal stress of ~ 20 MPa resulted in removal of one atomic layer of the carbide. This represents a new type of wear process, which differs from what one would predict from models based on fracture of brittle materials and what has been called atomic wear. For context, we compare the processes and conditions used to those relevant for metal-on-metal hip implants, concluding that these severe wear processes are probably not important for the head/cup junction but could be relevant to fretting wear and corrosion at modular junctions.

Keywords In situ · Transmission electron microscopy · Wear · Single asperity · Layer-by-layer · Carbide

Electronic supplementary material The online version of this article (doi:10.1007/s11249-015-0567-5) contains supplementary material, which is available to authorized users.

✉ Yifeng Liao
Yifeng.Liao@gmail.com; Yifeng.Liao@dowcorning.com

¹ Department of Materials Science and Engineering,
Northwestern University, Evanston, IL 60208, USA

1 Introduction

Wear and friction are fundamental phenomena in which one solid surface moves over another solid surface. These processes affect a broad range of tribological systems, ranging from engines to medical implants. About one-third of the global energy consumption is wasted by friction, while wear is a major component of maintenance, repair and breakdown costs [1, 2].

While many tribological theories at the macroscopic scale have been developed in the past century, knowledge of wear, particularly what takes place at single asperity contact at the nanoscale to submicron scale, is still very limited. Current classical wear mechanisms [1, 2], e.g., adhesive wear, attribute wear to crack initiation/propagation in the subsurface region (tens of nanometers to microns away from the surface, depending on the asperity geometry) based on contact mechanics considering plastic and/or elastic deformation [3]. For mild wear, it is often conjectured that fracture is aided by surface oxidization [4]. These mechanisms, however, often contradict the fact that wear can take place under very mild loads and that cracks can be initiated at both the surface and subsurface [5]. The difficulty of understanding wear processes is due in large part to the lack of direct imaging data for both the surface and subsurface during sliding. Conventional post facto investigations of the worn surface and wear debris rarely fully reveal the dynamics of frictional events and, in some cases, could be misleading. This is particularly true when characterizing the material buried in the surface by examining a cross-sectional specimen. The destructive sample preparation processes, usually involving cutting or etching, can destroy the original structure and introduce artifacts.

Recent advances in real-time single asperity probing techniques have provided fruitful insights into tribological processes at the nanoscale [6]. For instance, it has been directly observed that the carbon sp^3 -to- sp^2 transition is accelerated in wet sliding of a tungsten tip against diamond-like carbon films [7], while Jacobs and Carpick slid a silicon tip on diamond in situ inside a TEM and reported atom-by-atom wear [8]. In order to better understand the wear processes of hard materials, we exploit here an atomic force microscope (AFM)–transmission electron microscope (TEM) apparatus to mimic single asperity sliding on $M_{23}C_6$ (M: Co, Cr, Mo) carbides in a cast cobalt-chrome-molybdenum (CoCrMo) alloy; see [9–12] and references therein for further details about the $M_{23}C_6$ phase. The material was chosen because CoCrMo has been extensively used in tribological systems such as medical implants due to its excellent strength, fracture toughness and corrosion resistance. Cast CoCrMo has an fcc metastable matrix along with nanostructured $M_{23}C_6$ -type carbide precipitates, which act as strength enhancers and are critical to the wear performance, and also effects the mechanical properties. One important medical issue is that wear in vivo produces a large number of nanoparticles, which increase the metal ion level in patients [13, 14]. Although there has been substantial analysis using traditional macroscopic simulator tests [15–17], the wear mechanisms, particularly for the hard carbide phase, are not fully understood. We find here that a somewhat unexpected process takes place, namely removal of single layers of the hard $M_{23}C_6$ phase. This can be understood in terms of dislocation movement one plane below the surface, which is consistent with established interface dislocation models and a friction analysis based upon this [18], but very different from models that involve crack propagation.

2 Experimental

2.1 Materials

The materials were cut from a retrieved hip replacement made of high-carbon cast alloy (ASTM standard F75: Co–27Cr–6Mo, with ~ 0.3 wt % carbon) using an abrasive saw. The retrieved hip implant was explanted after 604 days of service. TEM thin foils were cut and transferred to a copper grid using an FEI Helios dual-beam focused ion beam (FIB) operated at 30 kV. The specimens were subsequently thinned to ~ 60 nm using 5–30 kV ions. As a final step, all TEM thin foils were cleaned using ion beam at 3 kV at -100 °C for 5 min in order to remove contamination.

2.2 In Situ AFM–TEM Sliding Setup

The copper grid holding the CoCrMo alloy was mounted on a tungsten rod and placed in a modified nanofactory TEM/AFM holder. The thin foils can move three dimensionally driven by a piezomotor with resolutions of 0.2 Å in XY and 0.025 Å in Z. An FEI Tecnai F20ST TEM at Argonne National Laboratory operated at 200 kV was employed for the in situ sliding tests. A silicon AFM tip fabricated on a cantilever was used as the sliding counterpart [19]. The experimental setup is shown in Fig. 1. The mechanical spring constant measured from the force–displacement curve was 5.2 N/m (see the method described in Ref. [19]), which is close to (~ 8 % less than) that calculated by the geometry of the cantilever (5.6 N/m, provided by the vendor). The lateral sliding speeds were set to ~ 200 nm/s. The processes were recorded using either a Gatan CCD camera or a TV-rate video camera. The normal force was determined from the displacement of the silicon tip from its rest position. After the in situ sliding tests, specimens were re-examined ex post facto using a JEOL 2100F TEM (200 kV) equipped with an electron energy loss spectrometer (EELS) at Northwestern University to check the composition of the wear debris. Videos of the in situ sliding tests are available in the Supplemental Information.

The AFM–TEM silicon tip was ~ 100 nm wide, so it was possible to slide selectively on the carbide precipitates. The compressive load was set to ~ 200 nN, equivalent to a normal pressure of ~ 20 MPa, given that the contact area was ~ 161 nm long and ~ 60 nm thick. The sliding distance was set to be similar to the length of the contact area and avoided sliding over the adjacent fcc matrix regions. Due to misalignment of the setup, an error of ~ 5 MPa is expected in the applied normal pressure. The normal load is about the same magnitude as the average pressure for hip implants [15]. The structural evolution at both the surface and subsurface was monitored in real time during sliding.

3 Results

Severe wear occurred at the carbide surface, while the silicon tip remained intact throughout the test. Figure 2a, b shows images of the carbide precipitate before and after the test, respectively. The geometry of the carbide after the test is shown by the white lines in Fig. 2a for comparison. The worn surface was determined to be $(51\bar{1})$ based on nano-beam electron diffraction results using the JEOL 2100 TEM as shown in Fig. 2c and the inset diffraction pattern. The thickness reduction for 250 passes was ~ 46 nm; thus, the wear rate (defined herein as thickness reduction per

Fig. 1 **a** Experiment setup of the in situ sliding test. The CoCrMo thin foil was made using conventional FIB methods. The spring constant of the cantilever when the silicon tip was attached was 5.2 N/m. **b** The boxed region at higher magnification showing the detailed contact region. Nanostructured carbide phases were present

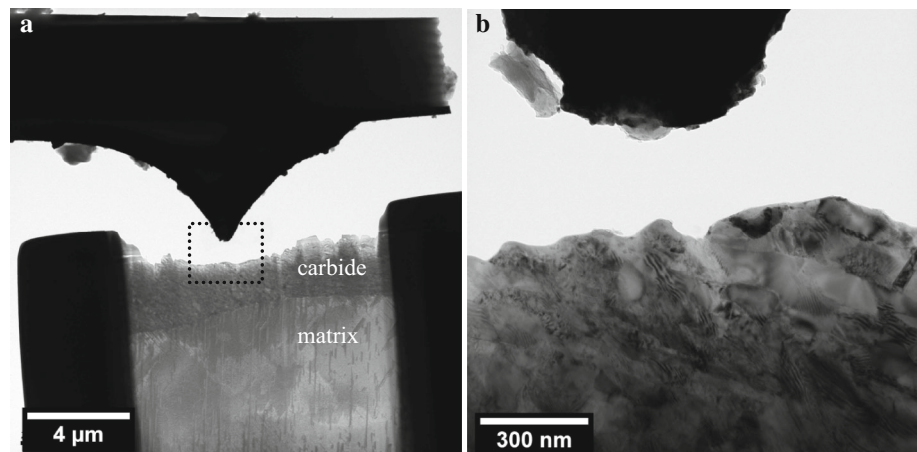
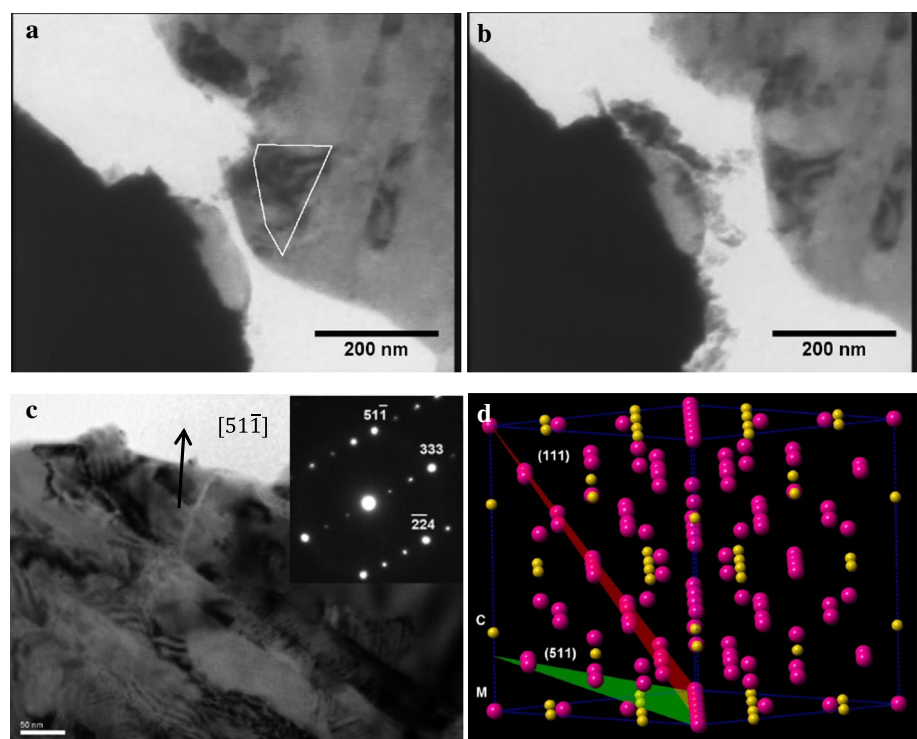


Fig. 2 **a** TEM micrograph of the tip/carbide prior to and **b** after the test. The geometry of the carbide after 250 sliding passes is marked in (a) by the white lines for comparison. The carbide surface plane is $(51\bar{1})$. **c** Bright-field micrograph of the carbide after the sliding test and **b** the corresponding diffraction pattern. The surface plane was $(51\bar{1})$. **d** Schematic of (111) and $(51\bar{1})$ plane in the $M_{23}C_6$ structure. The planes $\{51\bar{1}\}$ and $\{333\}$ have the highest structure factors for $M_{23}C_6$ structure, and their lattice spacings are identical [24]. The $(51\bar{1})$ highlighted in the figure is only slightly puckered and composed of metal atoms only, a feature similar to fcc (111) [74]



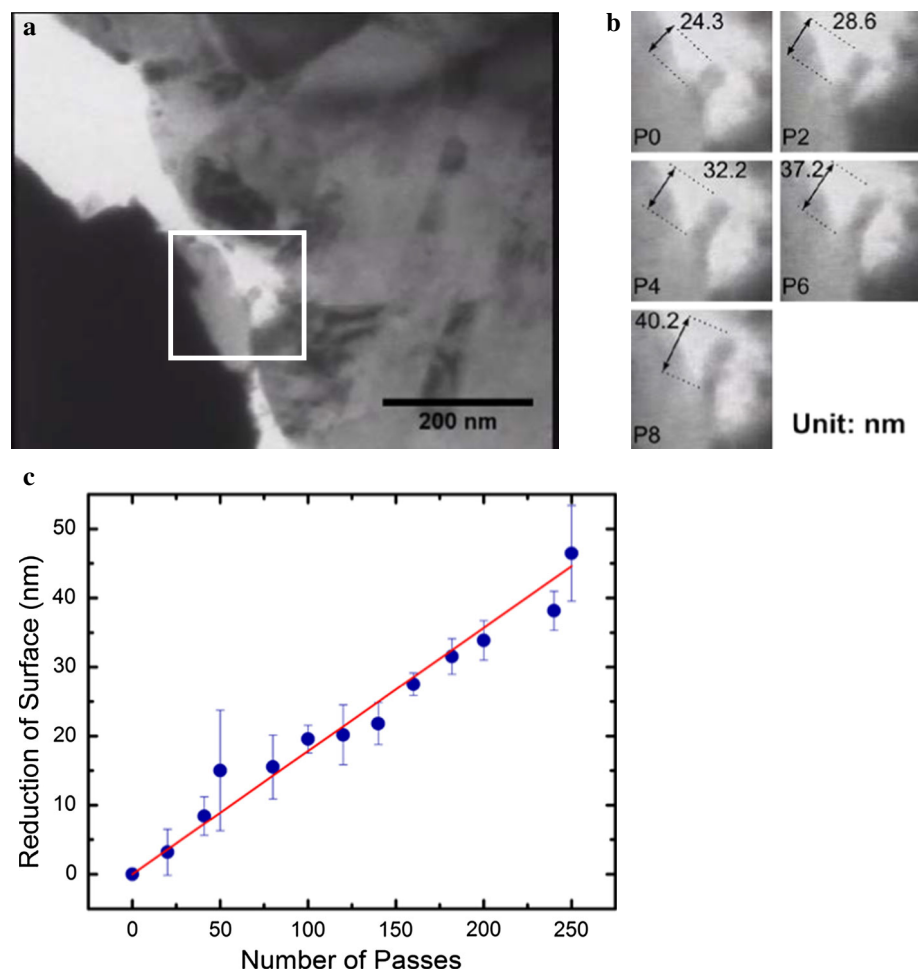
slide pass) was ~ 0.18 nm per pass. The reduction per slide pass wear is comparable to the $(51\bar{1})$ interplanar spacing of 0.20 nm [20], indicating that on average approximately one monolayer was removed for each sliding pass. In the carbide [21–23], $\{51\bar{1}\}$ has the same interplanar spacing as $\{111\}$ in the fcc matrix [24] and contains layers consisting of only metal atoms; thus, sliding on this plane can be favorable (see Fig. 2d).

Figure 3a, b shows the profile of the wear debris in the boxed region for eight consecutive passes with an interval of two passes. The length of the debris attached to the silicon tip consistently increased by 2.0 ± 0.4 nm for each pass, suggesting that the material removal was steady and

did not occur by a process involving cracks at the surface or subsurface. The volume increase in the debris shown was 335 ± 68 nm³ per pass (assuming the debris had a rod geometry with a diameter of 14.6 nm), which is about 14–21 % of the volume of the monolayer. The video can be found in Suppl. Video V1. Figure 3c shows the surface reduction as a function of time. Except before the 50th sliding pass in which the lower side of the surface was indented, the wear was linear. An animated video of the carbide phase imaged every 15–20 passes is provided in Suppl. Video V3 showing continuous wear of the surface.

No discernible dislocations were produced or fracture processes occurred; thus, fracture in the subsurface due to

Fig. 3 **a** Steady accumulation of the wear debris in the boxed region was monitored in the serial micrographs in **b** recorded with an interval of two sliding passes. The length (labeled) increased by ~ 2 nm for every single sliding pass. **c** Plot of the reduction of surface as a function of sliding passes. The wear rate was nearly linear and ~ 0.18 nm per sliding, which is close to the interplanar spacing of $(51\bar{1})$, suggesting that each slide pass removed one monolayer



the maximum shear stress based on contact mechanics (as has been suggested in the literature) does not account for the wear process in these experiments. It is worth noting that sliding on the CoCrMo fcc matrix in a separate experiment did create additional deformation in the sub-surface [25].

Figure 4a shows the profile of the tip and carbide after the sliding test recorded using the CCD camera. A number of nanoparticles of ~ 8 nm in diameter were generated, most of which were agglomerated on the silicon tip due to the large adhesion (discussed later). Figure 4b shows a HREM micrograph of a nanoparticle examined immediately after the sliding test, which was identified to be an $M_{23}C_6$ carbide based on the interplanar spacings and angles. No dislocations are present in the particle, suggesting that the particle had recrystallized as expected, similar to the observations by Shan et al. [26] in which a nickel submicron pillar was free of dislocations after indentation due to mechanical annealing. The post facto EELS data showed that the debris was composed of C, Co and Cr (the Mo peak was not examined as it overlaps with carbon); see Fig. 4c, d. No silicon was observed, indicating

that the carbide did not chemically react or mechanically mix with the silicon. Oxidation was also suppressed in the low vacuum environment as can be seen from the absence of the oxygen peak in the EELS spectrum. Similar wear particles of ~ 10 nm in diameter have been extensively observed in wear of metallic materials [4, 27, 28], but the generation of these nanoparticles has not been fully explained.

In contrast to the hard nature of the bulk carbide, the carbide wear debris appeared to be soft, presumably due to their small size [29], and could be further packed into larger particles, as shown in the serial TEM micrographs in Fig. 5. The debris, which is the same debris in Fig. 3a but after 18 passes, rolled up at the counterface to yield a particle of ~ 32 nm. For completeness, we note that the carbide debris did not cause discernible abrasion on either surface.

Strong adhesion played an important role in peeling of the monolayer and transferring nanodebris to the silicon tip. The long-range attractive forces were negligible when the silicon tip was ~ 10 nm from the carbide. The tip snapped into the carbide when it approached closer (see

Fig. 4 **a** The profile of the tip and the carbide after the sliding test (recorded using a CCD camera). Numerous wear debris nanoparticles of ~8 nm in diameter were generated and adhered to the silicon tip. **b** HREM micrograph of a typical wear debris nanoparticle identified to be $M_{23}C_6$ carbide. No dislocations were present in the particle. **c, d** EELS spectra of wear nanoparticle. **c** Carbon peak is present while no discernible silicon peak is observed. **d** Co and Cr peaks were present while oxygen was absent

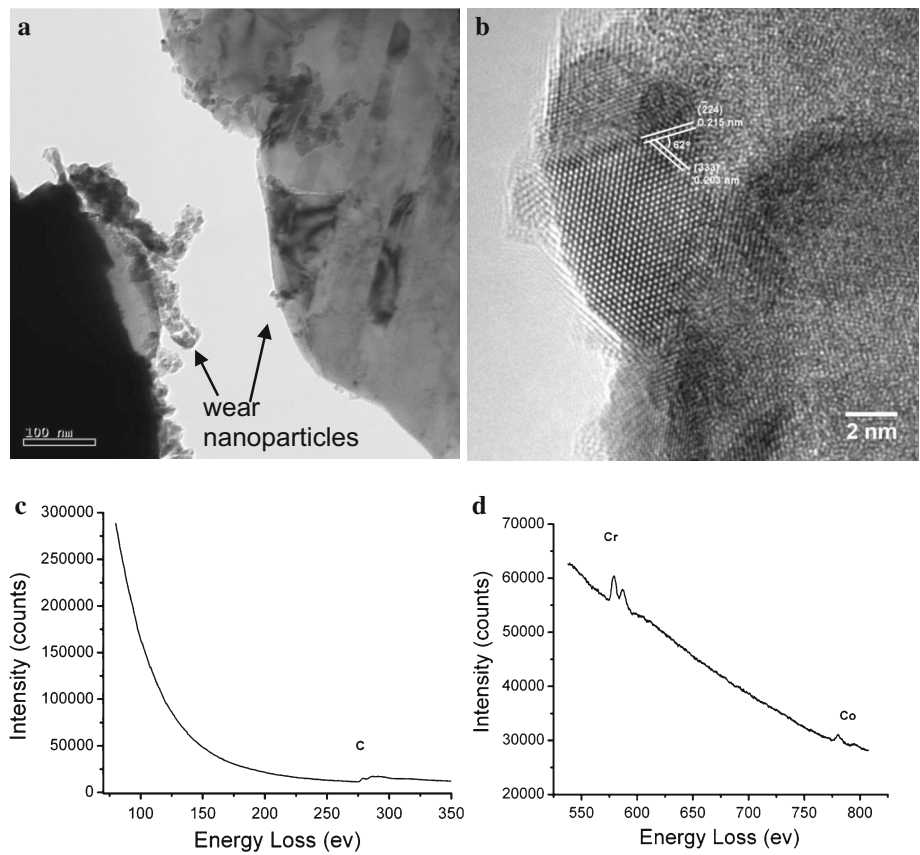


Fig. 5 **a** A loosely packed nanoparticle of 32 nm in diameter was formed at the counterface in the boxed region. **b** Serial micrographs showing that the particle was formed by rolling up the debris, which is the same one in Fig. 1c but after 18 sliding passes

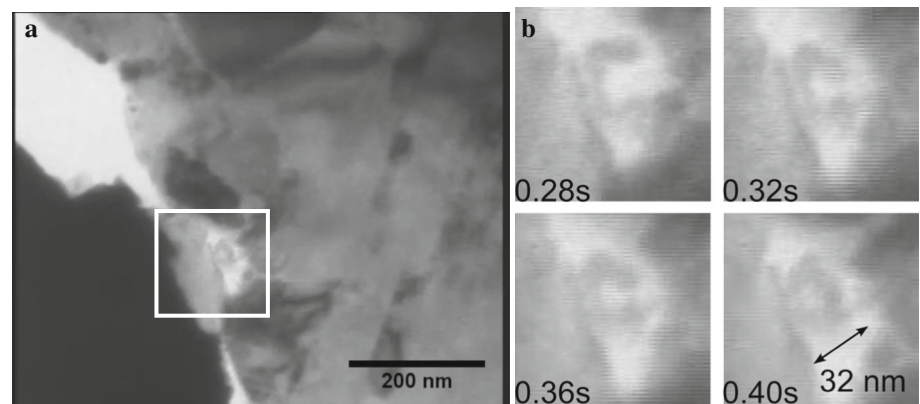


Fig. 6 **a** TEM micrograph taken right before snapping to contact. The critical separation between the silicon tip (bottom left) and the carbide (upper right) was ~10 nm. **b** The tip snapped onto the carbide when moved slightly closer

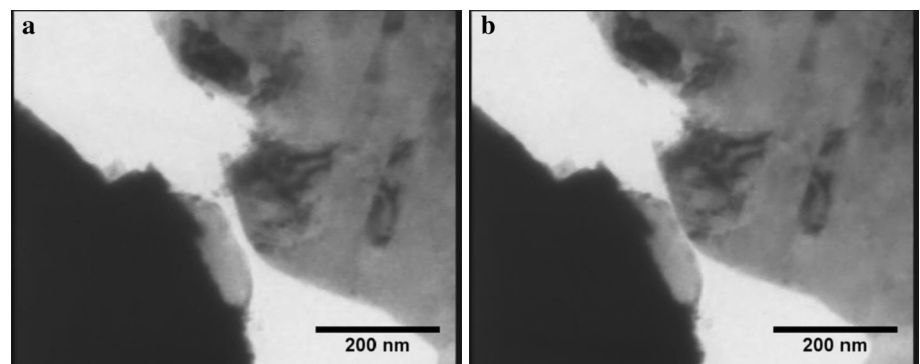


Fig. 6) because the adhesion built up so rapidly that the force gradient exceeded the spring constant of the cantilever (5.2 N/m). In order to examine the magnitude of the adhesion (defined as the force for separating the contacting surfaces herein), the specimen was retracted until it was detached from the tip, see Suppl. Video V2. Figure 7a, b shows TEM micrographs prior to and after the detachment, respectively. The tip was retracted by 186 ± 9 nm from its free position; thus, taking into the error of the spring constant ($\sim 8\%$), the adhesion force was calculated to be 967 ± 125 nN. Since the contact area was ~ 161 nm long and ~ 60 nm thick, the adhesion force per unit area was determined to be 100 ± 13 MPa, which is $\sim 20\%$ of the tensile yield stress of the bulk CoCrMo alloy (450–500 MPa [30]).

4 Discussion

4.1 Wear Coefficient and Adhesion

It is useful to work out the wear coefficient and the adhesive model that would be relevant for comparison with more macroscopic experiments and continuum models. Our previous nanoindentation tests using a diamond tip showed that the hardness of the $M_{23}C_6$ carbide was 15 GPa [9], and the reduced modulus $E_r^1 = 270$ GPa. From these measurements, the elastic modulus of the carbide E_c is given by [31]:

$$\frac{1}{E_r^1} = \frac{1 - \nu_d^2}{E_d} + \frac{1 - \nu_c^2}{E_c}$$

where E_d is the elastic modulus of diamond (1140 GPa); ν_d is the Poisson's ratio of diamond (0.07); and ν_c is the Poisson's ratio of the $M_{23}C_6$ carbide (which we will approximate as 0.3). The elastic modulus of the carbide can be calculated to be $E_c = 309$ GPa. The elastic modulus of silicon E_{Si} varies from 130 to 188 GPa with a typical value of 169 GPa [32].

The dimensionless wear coefficient K_c describes the relationship between the wear volume, normal load and hardness. It is given by [1]:

$$K_c = \frac{QH}{W}$$

where Q is the volume worn per unit distance, H the hardness (15 GPa) and W the applied load (~ 200 nN). For layer-by-layer wear,

$$Q = \text{Volume Lost/Sliding Distance} \\ = \frac{161 \times 60 \times 0.18}{161} \times 10^{-18} \text{ m}^2$$

The wear coefficient is calculated to be $K_c = 0.8$, suggesting that the wear is extremely severe if one transfers this rate to a macroscopic tribological application. (We note that it might be more appropriate to scale the wear rate by the fractional contact area of asperities for a bulk comparison.)

The adhesion mode can be determined using Maugis' parameter [33, 34]. For a Derjaguin–Muller–Toporov (DMT) model [34, 35], λ is less than 0.1, while for a Johnson–Kendall–Roberts (JKR) model, λ is greater 5. The adhesion is in the DMT–JKR transition model when $0.1 < \lambda < 5$.

The Maugis' parameter is given by [33]:

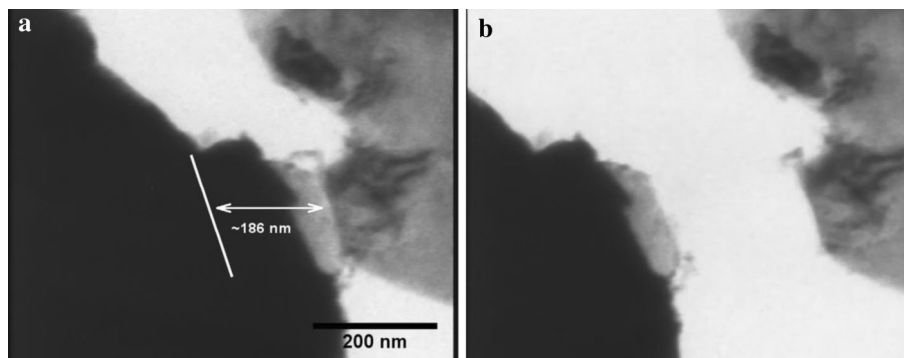
$$\lambda = 2\sigma_0 \left(\frac{R}{\pi\gamma K^2} \right)^{1/3}$$

where σ_0 is a constant adhesive stress; γ the work done by the adhesion $\gamma = \sigma_0 t$.

$$K = \frac{4}{3} \left(\frac{1 - \nu_c^2}{E_c} + \frac{1 - \nu_{Si}^2}{E_{Si}} \right)^{-1}$$

As described in the manuscript, $\sigma_0 = 100$ MPa, $t = \sim 10$ nm. The Poisson's ratio ν is ~ 0.3 and the radius is approximated to the contact length $R = 161$ nm. The Maugis' parameter is calculated to be ~ 0.03 , suggesting that the DMT model [35] applies. Note that the normal load refers to the applied normal load. The total normal load,

Fig. 7 **a** TEM micrograph showing the silicon tip attracted by the carbide due to the adhesion force. The rest position of the tip is marked by the white line. **b** The tip was detached from the carbide residing at the rest position



which is the sum of applied load and adhesion force, is not used as discussed in Ref. [34].

4.2 Wear Mechanism

We next turn to consider how our direct observations of the wear process compare to existing models. Microscopic wear of carbides and ceramics usually involves surface cracks [36] as indicted by tests in situ in an scanning electron microscope (SEM) [37–39]. For instance, Kitsunai and Hokkirigawa observed cracks with silicon carbide on the contact surface with increasing sliding cycles [38] and a change in the wear coefficients from 10^{-3} to 10^{-2} after ~ 15 cycles. However, we are dealing with much more severe wear with a wear coefficient of ~ 0.8 . As mentioned above, there was no evidence for subsurface plastic deformation, expected as the applied load was 2–3 orders of magnitude lower than the theoretical shear strength (tens of GPa) of the carbide. Similarly, the silicon tip is unlikely to accommodate any dislocations and did not show any wear. We therefore need to go beyond these models.

To explain our results, we now look at the mechanism responsible for monolayer wear. The carbide surface was subject to two friction forces, i.e., shearing at the junction and plowing in the sliding path [40]. For plowing, the indent depth into the silicon would be nearly twice of that in the carbide because the elastic modulus of silicon (169 GPa) is lower than that of the carbide (308 GPa). Therefore, one would expect more plowing of the silicon if this was the dominant wear mechanism, which is inconsistent with the experimental results. Thus, shearing at the junction dominates.

Sliding of the counterparts can take place via either the motion of the interface or motion of dislocations near the interface [18]. Motion of the interface would produce no severe wear in this case as there is no deformation in the subsurface. In contrast, motion of misfit dislocations at an interface will. These dislocations reside one layer below the interface when the lattice misfit is large [41, 42]. Sliding via motion of these misfit dislocations will transfer a single monolayer, consistent with the experimental results. For completeness, we note that classic approaches such as continuum plowing are consistent with atomistic models involving dislocation plasticity and interfacial sliding as recently shown [43].

4.3 Comparison to Atomistic Wear

It is appropriate to compare layer-by-layer wear to the atom-by-atom wear observed in AFM sliding tests [8, 44–46]. For instance, the wear of an AFM tip against a polymer substrate reported by Gotsmann and Lantz [44] was calculated to be ~ 1 atom per micron of sliding, and

Bhaskaran et al. [45] reported loss of ~ 1 atom per micron of sliding a silicon-containing diamond-like carbon tip. In the recent work by Jacobs and Carpick, the wear of silicon was severe and the volume removal rate varied from ~ 500 to 4000 nm^3 per micron of sliding [8]. While layer-by-layer wear shares some similarities with atom-by-atom wear (see [8, 44–46]), for instance the wear process is discrete with an atomistic activation volume, they are different wear mechanisms. Layer-by-layer wear involves collective removal of many atoms, and the shear stress is sufficient to remove the materials.

Some care is needed as the term atom-by-atom wear implies that single atoms are being removed sequentially, but the experimental data do not prove that this is always what was taking place. As sketched in Fig. 8, the issue is whether wear was taking place by the simultaneous collective breaking/changing of a large number of bonds similar to a martensitic transformation versus breaking/changing of single atomic structures similar to the motion of dislocations by the sequential movement of kinks. For a collective process, the activation volume will contain many atoms; for an atomistic process, it will be on the scale of a single atom. The experimental results of Jacobs et al. [47] indicate that for their experiments the activation volume was on the scale of atoms so was atomistic in character. However, this by itself does not prove that the process only involves detachment of single atoms, only that it is discretized at the atomic scale. For instance, a standard formulation for the energy to move a dislocation kink by a single discretized step is

$$E_P = \sigma_P b^2 a / \pi = \sigma_P V_{\text{act}} / \pi$$

where b is the Burgers vector, a the translation distance, E_P the Peierls energy and σ_P the Peierls stress. Here, the activation volume V_{act} is “atomistic” even though it is not simply a single-atom process. Indeed, Jacobs et al. [47] reference back to the dislocation approaches in their model. We note that this approach has been used to analyze thermally activated dislocation motion in the past, but as discussed by Hirth and Nix [48] there are complications with parameterizing the internal friction so it is not often used in the more recent literature.

While sharing many similarities, layer-by-layer is a different mechanism from atom-by-atom wear. Atom-by-atom wear is governed by stress-assisted thermally activated detachment of single atoms as shown in Ref. [8]. Layer-by-layer wear occurs via the sliding of interfacial dislocations (by single-atom kink migration) where the applied stress is sufficient to overcome the Peierls barrier. Thermal activation is less significant in layer-by-layer wear as the shear stresses are large. A comprehensive comparison of layer-by-layer and atom-by-atom wear is given in Table 1, which shows that the two mechanisms are different.

Fig. 8 **a** Schematic showing large volume activated in a sliding event in classic theories. **b** Single atom is activated in atomistic wear. Atoms in red are activated for wear

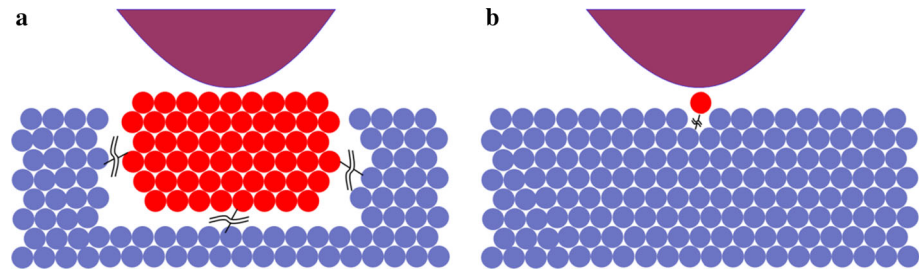


Table 1 Comparison of layer-by-layer and atom-by-atom wear mechanisms

Layer-by-layer wear	Atom-by-atom wear
<i>Discrete processes; activation volume close to atomic volume</i>	
Removal of many atoms	Removal of individual atoms
Shear stress dominated	Stress alone is insufficient to remove atoms
Materials removal by misfit dislocation motion	Materials removal by thermal activation
Flat worn surface with preferential orientation	Curved or flat surface conforming to the adhesion model
Severe wear	Ultra-low wear [44, 45] or severe wear [8]

4.4 Comparison to Metal Hip Replacement In Vivo/ In Vitro

Since the CoCrMo alloys are widely used for orthopedic devices, and in fact the specimen was from a retrieved metal-on-metal hip replacement, it is helpful to discuss briefly wear of CoCrMo alloys in vivo and in vitro in protein-contained fluids for context. It is known that wear and friction are extremely sensitive to the environment and are quite different when different types of proteins are present [49–51]. There have been a number of publications attempting to understand wear of CoCrMo hip replacement though in vivo and in vitro studies in simulated environments [52–58]. However, due to the technical impossibility of performing detailed in vivo studies since no viable animal model is currently known, many details are unknown. Even for in vitro studies, it is difficult to know all the details because it is very hard to probe buried interfaces.

One can be fairly positive that a passivation layer of surface oxide can be formed during the rubbing process; thus, the contact is probably that of oxide on an oxide layer [59, 60] for sliding of the head and cup, or for fretting wear at joints of modular implants. (To facilitate the surgical process, most current implant devices are comprised of a number of different metallic pieces which are hammered together while being surgically implanted, not welded together.) The oxide is probably Cr_2O_3 with Mo and Co going into the surrounding liquid. Metal-on-metal hip replacement bearings can generate carbonaceous film on the surface during sliding, which should provide some

lubrication and protection from corrosion [61–63]. We suspect that similar carbonaceous deposits form at fretting contacts, but to our knowledge this has not been explored. This carbonaceous material is relatively soft so could be penetrated by asperities leading to direct metal-on-carbide sliding similar to what is examined herein. For most cases, when the implants are working well the loads are not that high so there is unlikely to be much direct metal-on-metal or metal-on-carbide contact in the head–cup bearing.

However, everything may be different at the modular junctions. Here, there probably is direct metal on metal and metal on carbide, so the type of processes described herein may well be taking place in vivo. There is growing evidence, hinting that wear and corrosion at the modular junctions may be quite critical (e.g., [64–70]), so the processes described herein could be directly relevant to failure processes in vivo, although it would be premature to conclude this.

5 Summary

In summary, our in situ dry sliding test in vacuum shows that wear of the carbide in CoCrMo alloys can be achieved via monolayer-by-monolayer removal. The subsurface remained intact with no discernible dislocations or cracks. This represents a new type of wear process for hard materials and differs from the predictions from continuum-based mechanical models.

When will layer-by-layer wear occur? This is a complex question, which will depend upon the crystallography of

the two sliding bodies. Layer-by-layer wear will likely take place when there is an active slip system in the plane and slipping of monolayer is crystallographically favored in the two sliding bodies. The carbide phase usually does not have plasticity in its bulk form at the room temperature. Surfaces may behave differently, and plastic deformation is observed in this study. In our recent report [25], we showed chipping and plowing of cobalt fcc matrix in similar in situ TEM sliding tests, where the tests were sensitive to the attacking angle and conventional wear mechanisms dominated. Future investigation is needed to understand whether it will occur in other materials and test conditions.

One caveat is that the wear event is significantly influenced by the environment. The monolayer wear in this study is for silicon carbide dry sliding in vacuum. Other factors, such as the materials, lubrication by the tribological film [58, 63] and synovial fluid [16, 71–73], should be taken into account when modeling the wear mechanisms of an implant in service.

Acknowledgments This work was funded by the NSF under the Grant Number CMMI-1030703 and the NIH under the Grant Number 1RC2AR058993-01. The authors are indebted to Alfons Fischer for invaluable comments. Portions of this work were performed in the Electron Microscopy Center of the Center for Nanoscale Materials at Argonne National Laboratory, a US Department of Energy, Office of Science of Basic Energy Sciences User Facility under Contract No. DE-AC02-06CH11357.

References

- Hutchings, I.M.: *Tribology: Friction and Wear of Engineering Materials*. Edward Arnold, London (1992)
- Williams, J.A.: *Engineering Tribology*. Oxford University Press, New York (1994)
- Suh, N.P.: Overview of delamination theory of wear. *Wear* **44**(1), 1–16 (1977). doi:10.1016/0043-1648(77)90081-3
- Archard, J.F., Hirst, W.: An examination of a mild wear process. *Proc. R. Soc. A* **238**(1215), 515–528 (1957). doi:10.1098/rspa.1957.0015
- Rigney, D.A.: Comments on the sliding of wear of metals. *Tribol. Int.* **30**(5), 361–367 (1997). doi:10.1016/S0301-679x(96)00065-5
- Marks, L.D., Warren, O.L., Minor, A.M., Merkle, A.P.: Tribology in full view. *MRS Bull.* **33**(12), 1168–1173 (2008). doi:10.1557/mrs2008.247
- Mndange-Pfupfu, A., Ciston, J., Eryilmaz, O., Erdemir, A., Marks, L.D.: Direct observation of tribochemically assisted wear on diamond-like carbon thin films. *Tribol. Lett.* **49**(2), 351–356 (2013). doi:10.1007/s11249-012-0074-x
- Jacobs, T.D.B., Carpick, R.W.: Nanoscale wear as a stress-assisted chemical reaction. *Nat. Nanotechnol.* **8**(2), 108–112 (2013). doi:10.1038/nnano.2012.255
- Liao, Y., Pourzal, R., Stemmer, P., Wimmer, M.A., Jacobs, J.J., Fischer, A., Marks, L.D.: New insights into hard phases of CoCrMo metal-on-metal hip replacements. *J. Mech. Behav. Biomed.* **12**, 39–49 (2012). doi:10.1016/j.jmbbm.2012.03.013
- Liao, Y., Marks, L.D.: On the alignment for precession electron diffraction. *Ultramicroscopy* **117**, 1–6 (2012). doi:10.1016/j.ultramic.2012.03.021
- Liao, Y., Hoffman, E., Wimmer, M., Fischer, A., Jacobs, J., Marks, L.: CoCrMo metal-on-metal hip replacements. *Phys. Chem. Chem. Phys.* **15**(3), 746–756 (2013). doi:10.1039/c2cp42968c
- Stemmer, P., Pourzal, R., Liao, Y.F., Marks, L., Morlock, M., Jacobs, J.J., Wimmer, M.A., Fischer, A.: Microstructure of retrievals made from standard cast HC-CoCrMo alloys. *Metal. Metal. Total Hip Replace. Devices* **1560**, 251–267 (2013). doi:10.1520/Stp156020120033
- Jacobs, J.J., Skipor, A.K., Doorn, P.F., Campbell, P., Schmalzried, T.P., Black, J., Amstutz, H.C.: Cobalt and chromium concentrations in patients with metal on metal total hip replacements. *Clin. Orthop. Relat. Res.* **329**(Suppl), S256–S263 (1996)
- Silva, M., Heisel, C., Schmalzried, T.P.: Metal-on-metal total hip replacement. *Clin. Orthop. Relat. Res.* **430**, 53–61 (2005)
- Wimmer, M.A., Loos, J., Nassutt, R., Heitkemper, M., Fischer, A.: The acting wear mechanisms on metal-on-metal hip joint bearings: in vitro results. *Wear* **250**, 129–139 (2001). doi:10.1016/S0043-1648(01)00654-8
- Dowson, D., McNie, C.M., Goldsmith, A.A.J.: Direct experimental evidence of lubrication in a metal-on-metal total hip replacement tested in a joint simulator. *Proc. Int. Mech. Eng. C* **214**(1), 75–86 (2000). doi:10.1243/0954406001522822
- Sun, D., Wharton, J.A., Wood, R.J.K., Ma, L., Rainforth, W.M.: Microabrasion-corrosion of cast CoCrMo alloy in simulated body fluids. *Tribol. Int.* **42**(1), 99–110 (2009). doi:10.1016/j.triboint.2008.05.005
- Merkle, A.P., Marks, L.D.: A predictive analytical friction model from basic theories of interfaces, contacts and dislocations. *Tribol. Lett.* **26**(1), 73–84 (2007)
- Nafari, A., Karlen, D., Rusu, C., Svensson, K., Olin, H., Enoksson, P.: MEMS sensor for in situ TEM atomic force microscopy. *J. Microelectromech. Syst.* **17**(2), 328–333 (2008). doi:10.1109/Jmems.2007.912714
- Bowman, A.L., Arnold, G.P., Storms, E.K., Nereson, N.G.: The crystal structure of Cr₂₃C₆. *Acta Crystallogr. B* **28**(Oct15), 3102–3103 (1972)
- Maskiewicz, V.K., Williams, P.A., Prates, S.J., Bowsher, J.G., Clarke, I.C.: Characterization of protein degradation in serum-based lubricants during simulation wear testing of metal-on-metal hip prostheses. *J. Biomed. Mater. Res. B Appl. Biomater.* **94**(2), 429–440 (2010). doi:10.1002/jbm.b.31671
- Yan, Y., Neville, A., Dowson, D.: Biotribocorrosion—an appraisal of the time dependence of wear and corrosion interactions: II. Surface analysis. *J. Phys. D Appl. Phys.* **39**(15), 3206–3212 (2006). doi:10.1088/0022-3727/39/15/S11
- Heuberger, M.P., Widmer, M.R., Zobeley, E., Glockshuber, R., Spencer, N.D.: Protein-mediated boundary lubrication in arthroplasty. *Biomaterials* **26**(10), 1165–1173 (2005). doi:10.1016/j.biomaterials.2004.05.020
- Gaytan, S.M., Murr, L.E., Martinez, E., Martinez, J.L., Machado, B.I., Ramirez, D.A., Medina, F., Collins, S., Wicker, R.B.: Comparison of microstructures and mechanical properties for solid and mesh cobalt-base alloy prototypes fabricated by electron beam melting. *Metall. Mater. Trans. A* **41a**(12), 3216–3227 (2010). doi:10.1007/s11661-010-0388-y
- Liao, Y., Hoffman, E., Marks, L.: Nanoscale abrasive wear of CoCrMo in In Situ TEM sliding. *Tribol. Lett.* **57**(3), 1–6 (2015). doi:10.1007/s11249-015-0471-z
- Shan, Z.W., Mishra, R.K., Syed Asif, S.A., Warren, O.L., Minor, A.M.: Mechanical annealing and source-limited deformation in submicrometre-diameter Ni crystals. *Nat. Mater.* **7**(2), 115–119 (2008). doi:10.1038/nmat2085
- Burwell, J.T., Strang, C.D.: Metallic wear—discussion. *Proc. R. Soc. A* **212**(1111), 470–477 (1952)
- Don, J., Rigney, D.A.: Prediction of debris flake thickness. *Wear* **105**(1), 63–72 (1985). doi:10.1016/0043-1648(85)90006-7

29. Meyers, M.A., Mishra, A., Benson, D.J.: Mechanical properties of nanocrystalline materials. *Prog. Mater. Sci.* **51**(4), 427–556 (2006). doi:[10.1016/j.pmatsci.2005.08.003](https://doi.org/10.1016/j.pmatsci.2005.08.003)
30. Brunski, J.B.: *BioMaterials Science: an Introduction to Materials in Medicine*, 2nd edn. Elsevier, New York (2004)
31. Oliver, W.C., Pharr, G.M.: An improved technique for determining hardness and elastic-modulus using load and displacement sensing indentation experiments. *J. Mater. Res.* **7**(6), 1564–1583 (1992). doi:[10.1557/Jmr.1992.1564](https://doi.org/10.1557/Jmr.1992.1564)
32. Hopcroft, M.A., Nix, W.D., Kenny, T.W.: What is the young's modulus of silicon? *J. Microelectromech. Syst.* **19**(2), 229–238 (2010)
33. Maugis, D.: Adhesion of spheres—the Jkr-Dmt transition using a Dugdale model. *J. Colloid Interface Sci.* **150**(1), 243–269 (1992)
34. Grierson, D.S., Flater, E.E., Carpick, R.W.: Accounting for the JKR-DMT transition in adhesion and friction measurements with atomic force microscopy. *J. Adhes. Sci. Technol.* **19**(3–5), 291–311 (2005). doi:[10.1163/1568561054352685](https://doi.org/10.1163/1568561054352685)
35. Derjaguin, B.V., Muller, V.M., Toporov, Y.P.: Effect of contact deformations on adhesion of particles. *J. Colloid Interface Sci.* **53**(2), 314–326 (1975)
36. Miyoshi, K., Buckley, D.H.: The generation and morphology of single-crystal silicon-carbide wear particles under adhesive conditions. *Wear* **67**(3), 303–319 (1981). doi:[10.1016/0043-1648\(81\)90044-2](https://doi.org/10.1016/0043-1648(81)90044-2)
37. Kitsunai, H., Hokkirigawa, K., Tsumaki, N., Kato, K.: Transitions of microscopic wear mechanism for Cr₂O₃ ceramic coatings during repeated sliding observed in a scanning electron-microscope tribosystem. *Wear* **151**(2), 279–289 (1991). doi:[10.1016/0043-1648\(91\)90255-5](https://doi.org/10.1016/0043-1648(91)90255-5)
38. Kitsunai, H., Hokkirigawa, K.: Transitions of microscopic wear mode of silicon-carbide coatings by chemical-vapor-deposition during repeated sliding observed in a scanning electron-microscope tribosystem. *Wear* **185**(1–2), 9–15 (1995). doi:[10.1016/0043-1648\(94\)06580-2](https://doi.org/10.1016/0043-1648(94)06580-2)
39. Kato, K.: Micromechanisms of wear—wear modes. *Wear* **153**(1), 277–295 (1992). doi:[10.1016/0043-1648\(92\)90274-C](https://doi.org/10.1016/0043-1648(92)90274-C)
40. Bowden, F.P., Moore, A.J.W., Tabor, D.: The ploughing and adhesion of sliding metals. *J. Appl. Phys.* **80**, 80–91 (1942)
41. Shilkrot, L.E., Srolovitz, D.J.: Elastic analysis of finite stiffness bimaterial interfaces: Application to dislocation-interface interactions. *Acta Mater.* **46**(9), 3063–3075 (1998). doi:[10.1016/S1359-6454\(97\)00495-3](https://doi.org/10.1016/S1359-6454(97)00495-3)
42. Mader, W., Knauss, D.: Equilibrium position of misfit dislocations at planar interfaces. *Acta Metall. Mater.* **40**, S207–S215 (1992)
43. M'Ndange-Pfupfu, A., Marks, L.D.: A dislocation-based analytical model for the nanoscale processes of shear and plowing friction. *Tribol. Lett.* **39**(2), 163–167 (2010). doi:[10.1007/s11249-010-9629-x](https://doi.org/10.1007/s11249-010-9629-x)
44. Gotsmann, B., Lantz, M.A.: Atomistic wear in a single asperity sliding contact. *Phys. Rev. Lett.* **101**(12), 125501–125504 (2008)
45. Bhaskaran, H., Gotsmann, B., Sebastian, A., Drechsler, U., Lantz, M.A., Despont, M., Jaroenapibal, P., Carpick, R.W., Chen, Y., Sridharan, K.: Ultralow nanoscale wear through atom-by-atom attrition in silicon-containing diamond-like carbon. *Nat. Nanotechnol.* **5**(3), 181–185 (2010). doi:[10.1038/Nnano.2010.3](https://doi.org/10.1038/Nnano.2010.3)
46. Gnecco, E., Bennewitz, R., Meyer, E.: Abrasive wear on the atomic scale. *Phys. Rev. Lett.* **88**(21) (2002)
47. Jacobs, T.D.B., Gotsmann, B., Lantz, M.A., Carpick, R.W.: On the application of transition state theory to atomic-scale wear. *Tribol. Lett.* **39**(3), 257–271 (2010). doi:[10.1007/s11249-010-9635-z](https://doi.org/10.1007/s11249-010-9635-z)
48. Hirth, J.P., Nix, W.D.: An analysis of thermodynamics of dislocation glide. *Phys. Status Solidi* **35**(1), 177–188 (1969). doi:[10.1002/pssb.19690350116](https://doi.org/10.1002/pssb.19690350116)
49. Mathew, M.T., Nagelli, C., Pourzal, R., Fischer, A., Laurent, M.P., Jacobs, J.J., Wimmer, M.A.: Tribolayer formation in a metal-on-metal (MoM) hip joint: an electrochemical investigation. *J. Mech. Behav. Biomed.* **29**, 199–212 (2014). doi:[10.1016/j.jmbbm.2013.08.018](https://doi.org/10.1016/j.jmbbm.2013.08.018)
50. Munoz, A.I., Mischler, S.: Effect of the environment on wear ranking and corrosion of biomedical CoCrMo alloys. *J. Mater. Sci. Mater. Med.* **22**(3), 437–450 (2011). doi:[10.1007/s10856-010-4224-0](https://doi.org/10.1007/s10856-010-4224-0)
51. Yan, Y., Neville, A., Blowson, D.: Biotribocorrosion of CoCrMo orthopaedic implant materials—assessing the formation and effect of the biofilm. *Tribol. Int.* **40**(10–12), 1492–1499 (2007). doi:[10.1016/j.triboint.2007.02.019](https://doi.org/10.1016/j.triboint.2007.02.019)
52. Billi, F., Benya, P., Kavanaugh, A., Adams, J., McKellop, H., Ebramzadeh, E.: The John Charnley Award: an accurate and extremely sensitive method to separate, display, and characterize wear debris: part 2: metal and ceramic particles. *Clin. Orthop. Relat. Res.* **470**(2), 339–350 (2012). doi:[10.1007/s11999-011-2058-9](https://doi.org/10.1007/s11999-011-2058-9)
53. Buscher, R., Fischer, A.: The pathways of dynamic recrystallization in all-metal hip joints. *Wear* **259**, 887–897 (2005). doi:[10.1016/j.wear.2005.02.036](https://doi.org/10.1016/j.wear.2005.02.036)
54. Lappalainen, R., Selenius, M., Anttila, A., Kontinen, Y.T., Santavirta, S.S.: Reduction of wear in total hip replacement prostheses by amorphous diamond coatings. *J. Biomed. Mater. Res. B Appl. Biomater.* **66**(1), 410–413 (2003). doi:[10.1002/jbm.b.10026](https://doi.org/10.1002/jbm.b.10026)
55. Firkins, P.J., Tipper, J.L., Saadatzadeh, M.R., Ingham, E., Stone, M.H., Farrar, R., Fisher, J.: Quantitative analysis of wear and wear debris from metal-on-metal hip prostheses tested in a physiological hip joint simulator. *Biomed. Mater. Eng.* **11**(2), 143–157 (2001)
56. Tipper, J.L., Firkins, P.J., Ingham, E., Fisher, J., Stone, M.H., Farrar, R.: Quantitative analysis of the wear and wear debris from low and high carbon content cobalt chrome alloys used in metal on metal total hip replacements. *J. Mater. Sci. Mater. Med.* **10**(6), 353–362 (1999). doi:[10.1023/A:1026473723777](https://doi.org/10.1023/A:1026473723777)
57. Chan, F.W., Boby, J.D., Medley, J.B., Krygier, J.J., Tanzer, M.: The Otto Aufranc Award. Wear and lubrication of metal-on-metal hip implants. *Clin. Orthop. Relat. Res.* **369**, 10–24 (1999)
58. Wimmer, M.A., Sprecher, C., Hauert, R., Tager, G., Fischer, A.: Tribochemical reaction on metal-on-metal hip joint bearings—a comparison between in vitro and in vivo results. *Wear* **255**, 1007–1014 (2003). doi:[10.1016/S0043-1648\(03\)00127-3](https://doi.org/10.1016/S0043-1648(03)00127-3)
59. Yan, Y., Neville, A., Dowson, D.: Biotribocorrosion—an appraisal of the time dependence of wear and corrosion interactions: I. The role of corrosion. *J. Phys. D Appl. Phys.* **39**(15), 3200–3205 (2006). doi:[10.1088/0022-3727/39/15/S10](https://doi.org/10.1088/0022-3727/39/15/S10)
60. Yan, Y., Neville, A., Dowson, D.: Tribo-corrosion properties of cobalt-based medical implant alloys in simulated biological environments. *Wear* **263**, 1105–1111 (2007). doi:[10.1016/j.wear.2007.01.114](https://doi.org/10.1016/j.wear.2007.01.114)
61. Pourzal, R., Martin, E.J., Vajpayee, S., Liao, Y., Wimmer, M.A., Shull, K.R.: Investigation of the role of tribofilms in self-mating CoCrMo systems utilizing a quartz crystal microtribometer. *Tribol. Int.* **72**, 161–171 (2014). doi:[10.1016/j.triboint.2013.12.015](https://doi.org/10.1016/j.triboint.2013.12.015)
62. Martin, E.J., Pourzal, R., Mathew, M.T., Shull, K.R.: Dominant role of molybdenum in the electrochemical deposition of biological macromolecules on metallic surfaces. *Langmuir* **29**(15), 4813–4822 (2013). doi:[10.1021/la304046q](https://doi.org/10.1021/la304046q)
63. Liao, Y., Pourzal, R., Wimmer, M.A., Jacobs, J.J., Fischer, A., Marks, L.D.: Graphitic tribological layers in metal-on-metal hip replacements. *Science* **334**(6063), 1687–1690 (2011). doi:[10.1126/science.1213902](https://doi.org/10.1126/science.1213902)
64. John Cooper, H., Della Valle, C.J., Berger, R.A., Tetreault, M., Paprosky, W.G., Sporer, S.M., Jacobs, J.J.: Corrosion at the head-

- neck taper as a cause for adverse local tissue reactions after total hip arthroplasty. *J. Bone Joint Surg.* **94**(18), 1655–1661 (2012). doi:[10.2106/jbjs.k.01352](https://doi.org/10.2106/jbjs.k.01352)
65. Gilbert, J.L., Sivan, S., Liu, Y., Kocagoz, S.B., Arnholt, C.M., Kurtz, S.M.: Direct in vivo inflammatory cell-induced corrosion of CoCrMo alloy orthopedic implant surfaces. *J. Biomed. Mater. Res. A* (2014). doi:[10.1002/jbm.a.35165](https://doi.org/10.1002/jbm.a.35165)
66. Cooper, H.J., Urban, R.M., Wixson, R.L., Meneghini, R.M., Jacobs, J.J.: Adverse local tissue reaction arising from corrosion at the femoral neck-body junction in a dual-taper stem with a cobalt-chromium modular neck. *J. Bone Joint Surg. Am.* **95**(10), 865–872 (2013). doi:[10.2106/JBJS.L.01042](https://doi.org/10.2106/JBJS.L.01042)
67. Whitehouse, M.R., Endo, M., Masri, B.A.: Adverse local tissue reaction associated with a modular hip hemiarthroplasty. *Clin. Orthop. Relat. Res.* **471**(12), 4082–4086 (2013). doi:[10.1007/s11999-013-3133-1](https://doi.org/10.1007/s11999-013-3133-1)
68. Jacobs, J.J., Cooper, H.J., Urban, R.M., Wixson, R.L., Della Valle, C.J.: What do we know about taper corrosion in total hip arthroplasty? *J. Arthroplasty* **29**(4), 668–669 (2014). doi:[10.1016/j.arth.2014.02.014](https://doi.org/10.1016/j.arth.2014.02.014)
69. Nassif, N.A., Nawabi, D.H., Stoner, K., Elpers, M., Wright, T., Padgett, D.E.: Taper design affects failure of large-head metal-on-metal total hip replacements. *Clin. Orthop. Relat. Res.* **472**(2), 564–571 (2014). doi:[10.1007/s11999-013-3115-3](https://doi.org/10.1007/s11999-013-3115-3)
70. Pivec, R., Meneghini, R.M., Hozack, W.J., Westrich, G.H., Mont, M.A.: Modular taper junction corrosion and failure: how to approach a recalled total hip arthroplasty implant. *J. Arthroplasty* **29**(1), 1–6 (2014). doi:[10.1016/j.arth.2013.08.026](https://doi.org/10.1016/j.arth.2013.08.026)
71. Scholes, S.C., Unsworth, A., Hall, R.M., Scott, R.: The effects of material combination and lubricant on the friction of total hip prostheses. *Wear* **241**(2), 209–213 (2000). doi:[10.1016/S0043-1648\(00\)00377-X](https://doi.org/10.1016/S0043-1648(00)00377-X)
72. Wang, F.C., Brockett, C., Williams, S., Udofia, I., Fisher, J., Jin, Z.M.: Lubrication and friction prediction in metal-on-metal hip implants. *Phys. Med. Biol.* **53**(5), 1277–1293 (2008). doi:[10.1088/0031-9155/53/5/008](https://doi.org/10.1088/0031-9155/53/5/008)
73. Mavraki, A., Cann, P.M.: Lubricating film thickness measurements with bovine serum. *Tribol. Int.* **44**(5), 550–556 (2011). doi:[10.1016/j.triboint.2010.07.008](https://doi.org/10.1016/j.triboint.2010.07.008)
74. Double, D.D., Zambelli, G.: Microstructure and crystallography of directionally solidified (Co, Ni)-Cr23c6 eutectic alloy. *J. Mater. Sci.* **13**(3), 534–540 (1978). doi:[10.1007/Bf00541803](https://doi.org/10.1007/Bf00541803)